Transformation Path Dependence of the Bain Strain Relaxation during Decomposition of a Hypereutectoid CuBe Alloy

B. CHEONG, K. HONO, and D.E. LAUGHLIN

A transmission electron microscopy (TEM) investigation is conducted to study the relaxation of the Bain transformation strain during decomposition of a Be-rich hypereutectoid CuBe alloy. The relaxation is found to occur mainly through two basic mechanisms; habit plane rotation and the formation of a polytwin morphology. Depending on the path of the initial stages of the decomposition, these two mechanisms interplay in different ways to give rise to two different kinds of precipitate morphologies. For quenched and aged alloys, the relaxation process involves global habit plane rotation of single-domain plates along with a reconfiguration into a macroscopic polytwin morphology. For air-cooled alloys, the relaxation process involves the formation of sawtooth type polytwin plates characterized by a segment-wise habit plane rotation. A few questions which resulted from the experiments are considered by analysis of the elastic strain energy of a polytwin plate. It is suggested that the sawtooth morphology is a metastable morphology which does not satisfy the invariant plane strain condition and which comes about through certain kinetic effects under the influence of the elastic instability of the intermediate α' face-centered tetragonal (fct) state.

I. INTRODUCTION

DECOMPOSITION of a hypereutectoid β(bcc) phase CuBe alloy into the two-phase [γ(B2) + α(fcc)] mixture[1,2] represents an interesting class of phase transformations in which diffusional atomic reconfiguration (composition separation and bcc to B2 atomic ordering) is accompanied by a large change in the crystal lattice (bcc to fcc). The abbreviations bcc and fcc represent body-centered cubic and face-centered cubic, respectively. Recently, the authors have performed a transmission electron microscopy (TEM) investigation[3] to study the relaxation of the Bain transformation strain associated with the bcc to fcc crystal lattice rearrangement with particular regard to potential synergistic interplay with diffusional atomic reconfiguration processes. Focus was placed on the as-quenched states in which many characteristic events are already occurring due to the remarkably rapid kinetics of the decomposition. A distinct mechanism of the transformation strain relaxation was observed which involves the development of the polytwin precipitate plates of a characteristic sawtooth morphology. The morphology was examined in terms of a formation mechanism and it was suggested that both diffusional and diffusionless atomic motions may be necessary for its formation. Many interesting questions remain to be answered concerning the thermodynamic and kinetic nature of the sawtooth morphology. In the present study, a few of these questions are explored by examining alloys prepared by two different heat treatments: air cooling and water quenching followed by aging. A problem that is addressed is whether the development of the sawtooth morphology is peculiar to a certain transformation path or, to put it in more general terms, how a change in transformation path would affect the relaxation of the Bain transformation strain and the precipitate morphology. Based on experimental results, the problem of the stability of a polytwin plate of the sawtooth morphology is considered.

B. CHEONG, Postdoctoral Associate, and D.E. LAUGHLIN, Professor, are with the Department of Materials Science and Engineering, Carnegie Mellon University, Pittsburgh, PA 15213. K. HONO, Research Associate, is with the Institute for Materials Research, Tohoku University, Sendai 980, Japan.

Manuscript submitted June 23, 1993.

II. THEORETICAL BACKGROUND

A portion of the CuBe phase diagram[4] is reproduced schematically in Figure 1(a) with relevant lines added and/or extrapolated. The critical line of the second-order A2 → B2 ordering transition is depicted as a dashed line. The dotted lines demarcate the conditional spinodals[5] in which spinodal decomposition is thermodynamically possible contingent upon A2 → B2 ordering. A chemical-free energy *vs* composition diagram is shown in Figure 1(b) which is consistent with the phase diagram characteristics at an arbitrary temperature T_A below the eutectoid temperature. The free energy of the γ(B2) phase plotted in the diagram is assumed to satisfy the extremization condition; $\partial F/\partial \eta|_c = 0$ at a given composition (c), where η is a long-range order parameter. According to these diagrams, a disordered β phase of the composition c^β, if supercooled to the temperature T_A, would decompose along the path A → B → C → D → E to produce the equilibrium α precipitates. The main events during the transformation are summarized in the following:

1. A → B: bcc to B2 atomic ordering;
2. B → C: isostructural decomposition leading to the formation of $\{001\}_\gamma$ Cu-rich Guinier-Preston (GP) zones;
3. C → D: crystal lattice rearrangement of $\{001\}_\gamma$ GP zones into $\{001\}_\gamma\alpha'$ (fct) precipitates; and
4. D → E: relaxation of the α' precipitates to the equilibrium α precipitates.

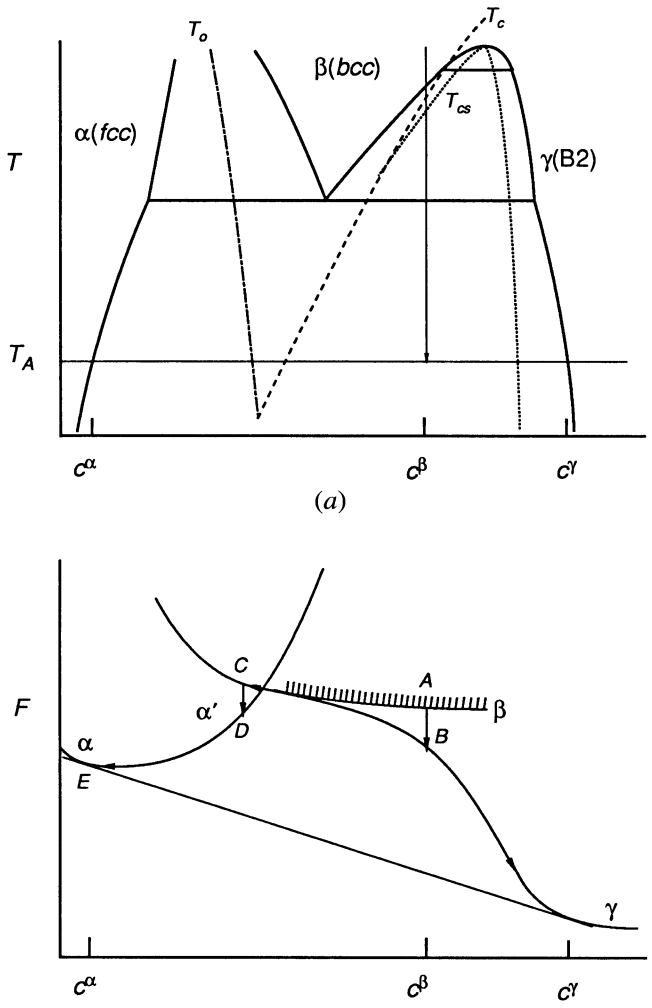

Fig. 1—(*a*) Schematic of the CuBe phase diagram (see text). (*b*) Chemical-free energy *vs* composition diagram consistent with the phase diagram characteristics at an arbitrary temperature T_A. When supercooled to T_A, a disordered β phase of the composition c^β would decompose along the path A → B → C → D → E to produce the equilibrium α (fcc) precipitates.

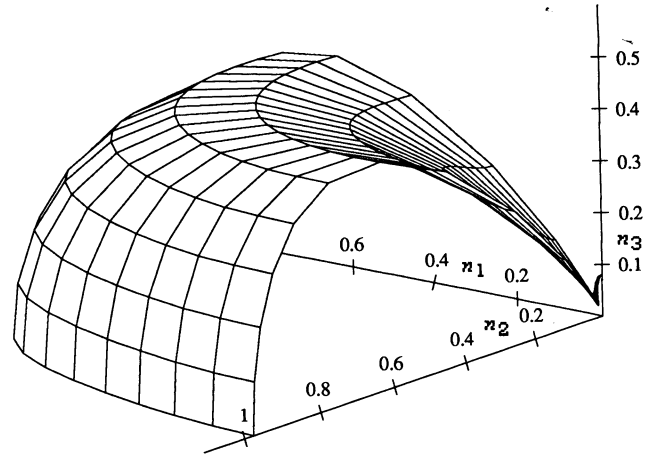

Fig. 2—An octant of the elastic energy surface as a function of habit plane normals of a fcc platelike precipitate embedded in the B2 matrix. Notice a local maximum along the [001] direction, indicating that the α' state is elastically unstable.

With regard to the relaxation of the Bain distortion, the following points are emphasized. First, the crystal lattice of the $\{001\}_\gamma$ Cu-rich GP zones due to step 2 is tetragonally elongated along the direction of its habit plane normal and this, in effect, accommodates a part of the Bain transformation strain even before step 3 commences. This point was first discussed by Khachaturyan and Laughlin[6] for the case of the decomposition of α (fcc) phase. Second, the α' precipitates resulting from step 3 are elastically unstable. This is illustrated in Figure 2 which represents the elastic strain energy of a constrained fcc platelike precipitate embedded in the B2 matrix as a function of habit plane normal. One can see a local maximum along the $[001]_\gamma$ direction which signifies instability. Due to this instability, further relaxation of the Bain transformation strain immediately sets in, contingent upon transition of the $\{001\}_\gamma$ GP zone to the α' state. Two possible paths may be envisioned from the graph: a precipitate plate may rotate the habit plane into a lower energy position while maintaining its single-domain entity and/or it may undergo a certain character change which might alter the relative stability of the $\{001\}_\gamma$ habit, *e.g.*, development of polytwin domains. It may be helpful to note the difference between the two heat-treatment schemes employed in the present work on this framework. As one can notice with the aid of the phase diagram, the air cooling process, in contrast to the quench/aging process, provides B2 ordered alloys with an extended reaction time of decomposition in the (B2 + bcc) two-phase state. This leads to a significant coarsening of the $\{001\}_\gamma$ GP zones before step 3 begins. One can expect that the rotation of the habit plane as a single-domain entity gets more difficult for a larger precipitate plate since it requires an extensive solute redistribution.

III. EXPERIMENTAL PROCEDURE

As-cast Cu-Be binary alloys containing 9.04 wt pct Be (41.2 at. pct Be) were provided by BrushWellman Inc. The as-received alloys were homogenized for 1 day at 840 °C and were sliced into plates about 0.5-mm thick. The specimens were then cold-rolled to thicknesses of about 0.2 mm. Due to the brittleness of the alloys, a further reduction in thickness was made by mechanical polishing. Discs of 3 mm in diameter were punched out from these specimens and were then given a disordering treatment for 1 hour at 840 °C. For each of these heat treatments, the specimens were encapsulated in argon backfilled quartz tubes. The disordered specimens were either quenched into iced-brine water or air-cooled to room temperature outside the furnace. Quenching of the disordered specimens was performed by rapidly transferring the tube and smashing it onto a heavy metal object which was immersed in the quenchant. Quenched specimens were encapsulated in argon backfilled pyrex tubes and were aged in a three-zone Lindberg furnace.

Specimens for TEM were prepared using a twin-jet electropolisher with an electrolyte of 70 vol pct methanol and 30 vol pct nitric acid below −30 °C and at 10 V.

When necessary, electropolished samples were ion-milled for short periods of time (<10 minutes) at 4 to 5 keV and 0.2 mA. The TEM was performed using a PHILIPS 420T* operating at 120 kV.

*PHILIPS 420T is a trademark of Philips Electronic Instruments Corp., Mahwah, NJ.

IV. RESULTS

A. *Air-Cooled State*

The main characteristics of the air-cooled state are depicted in a series of TEM photographs shown in Figure 3. In the bright-field (BF) micrograph a network of polytwin precipitate plates which are aligned along the [010] and [001] directions of the matrix γ phase and have a characteristic sawtooth morphology can be observed. The morphology is featured by rotation of the broader segments from the $[010]_\gamma$ or the $[001]_\gamma$ orientation that are regularly interspersed with thin segments in twin orientation. A set of thin twin segments is shown in the dark-field (DF) image taken with the precipitate reflection indicated in the selected area diffraction pattern (SADP) ($[100]_\gamma//[110]_{prec}$ zone axis pattern; see the schematic SADP in Figure 4(a) and the notation convention in Figure 4(b)). In a previous study,[3] it was proposed that the formation of thin twin domains initiates by the intersection or impingement of two orthogonal sets of plates. In that light, it is interesting to note that twice the spacing between thin twin domains, which may be taken as the average frequency of the impingement on one side of a plate, is comparable to the mean separation between two adjacent $\langle 001\rangle_\gamma$ plates.

Some information on the crystallography of the observed sawtooth morphology is as follows. From tilting experiments, it is found that the precipitate plates are edge-on along the $[100]_\gamma$ zone axis, meaning that the habit planes of broader domain segments are of the $\{0hk\}_\gamma$ type. By a trace analysis, these habit planes are determined for the variant $3\cdot1$ to be approximately $(031)_\gamma$ with a slight variation. This variation in habit planes can be clearly seen from the associated SADP shown in Figure 3(c) by the spread of the 002 ($3\cdot1$) precipitate reflections over a small range of angle. Both of these features indicate nonuniformity in the extent of strain relaxation among different segments of the variant $3\cdot1$.

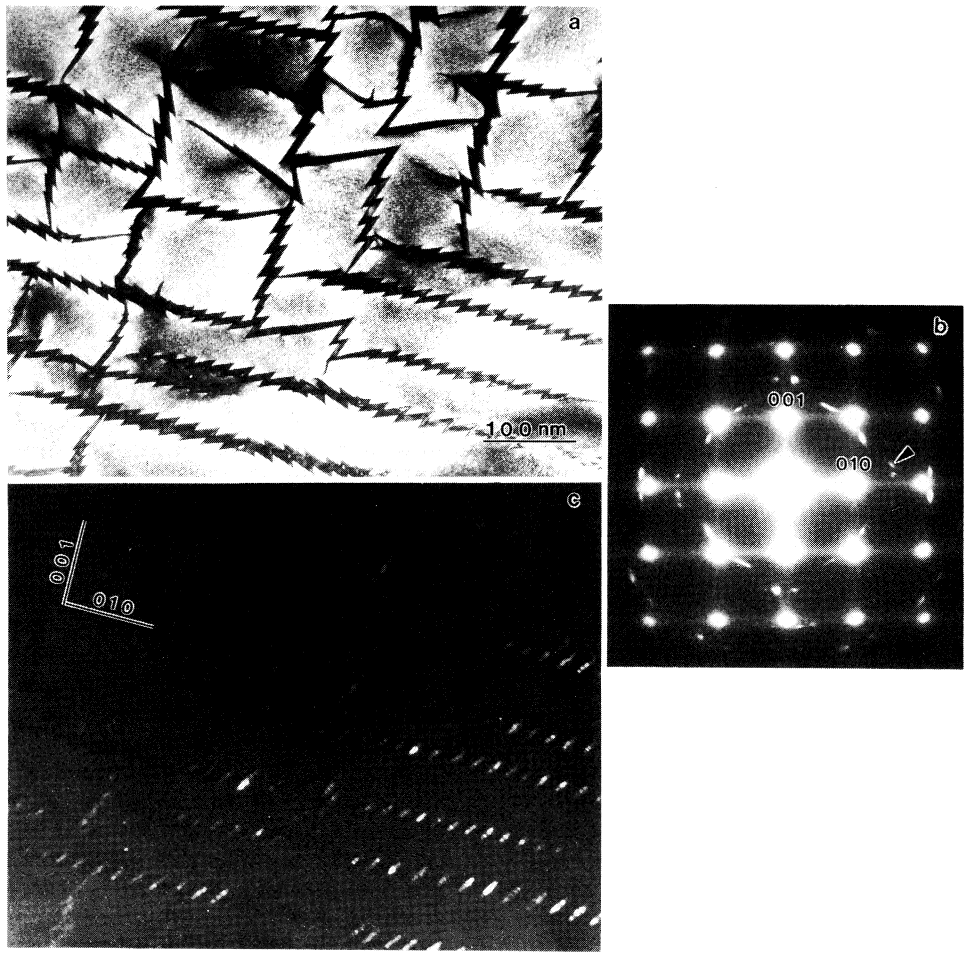

Fig. 3—TEM photographs showing the main characteristics of the air-cooled state. (*a*) BF image. (*b*) Associated SADP taken along the $[100]_\gamma//[110]_{prec}$ zone axis. (*c*) DF image taken with the precipitate reflection in (b). Note the $\langle 001\rangle_\gamma$ network of polytwin precipitate plates of a characteristic sawtooth morphology.

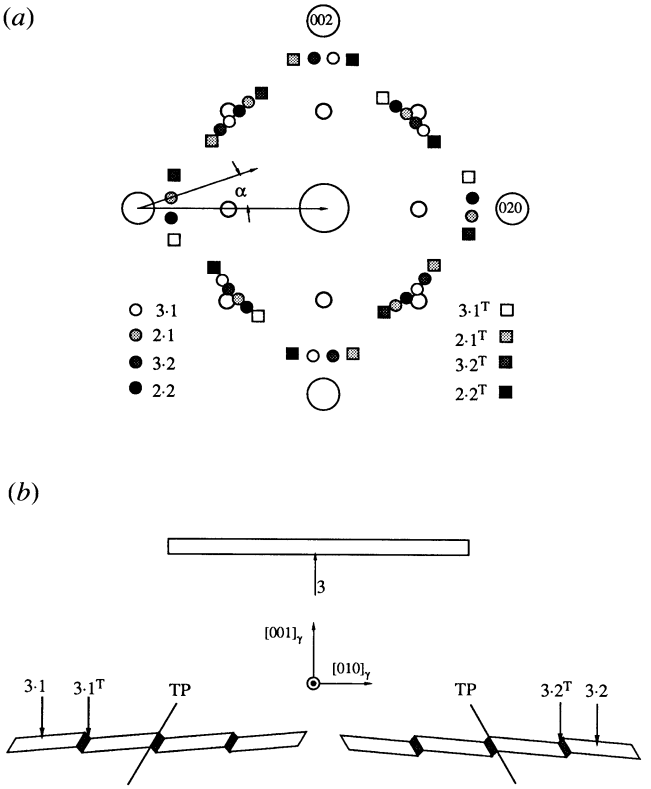

Fig. 4 — Schematics illustrating (*a*) the construction of the SADP shown in Figure 3(b) and (*b*) the sawtooth morphology with the notation convention used in (a). See text for a definition of the angle α. TP denotes twin plane.

The extent of the Bain strain relaxation was measured by determining the ratio $t = |\mathbf{g}^{\gamma}_{002}|/|\mathbf{g}^{\text{var3}\cdot 1}_{002}|$, where $\mathbf{g}$ is the reciprocal lattice vector. It is found to be about 0.90, which is significantly less than the equilibrium value 0.9425.

B. *Quenched and Aged State*

The Bain strain relaxation in aged states was examined in the alloys which were quenched and aged at 300 °C for 24 hours. Some selected features of the microstructures of the aged alloys are shown in Figures 5 and 6. We will first examine the overall appearance of the microstructures. The micrographs in Figure 5 show an array of individual precipitate plates, each having its respective habit plane rotated globally over the whole plate, in contradistinction to the characteristic feature of the air-cooled alloys (*i.e.*, well-developed sawtooth morphology). From tilting experiments, the habit planes are found to be once again of the $(0hk)_\gamma$ type, specifically $(031)_\gamma$ on average. Distinct as they are from the microstructures of the air-cooled alloys, the microstructures of the aged alloys often exhibit a characteristic spatial distribution of the precipitate plates in which regions of different *c*-axis variants are interweaved to form a macroscopic polytwin configuration. This is shown in the BF images of Figure 6. It is noticed that, as in the case of a polytwin plate, the boundaries between different regions run nearly parallel to the $\langle 110\rangle_\gamma$ directions. As is well known from studies of tweed microstructure,

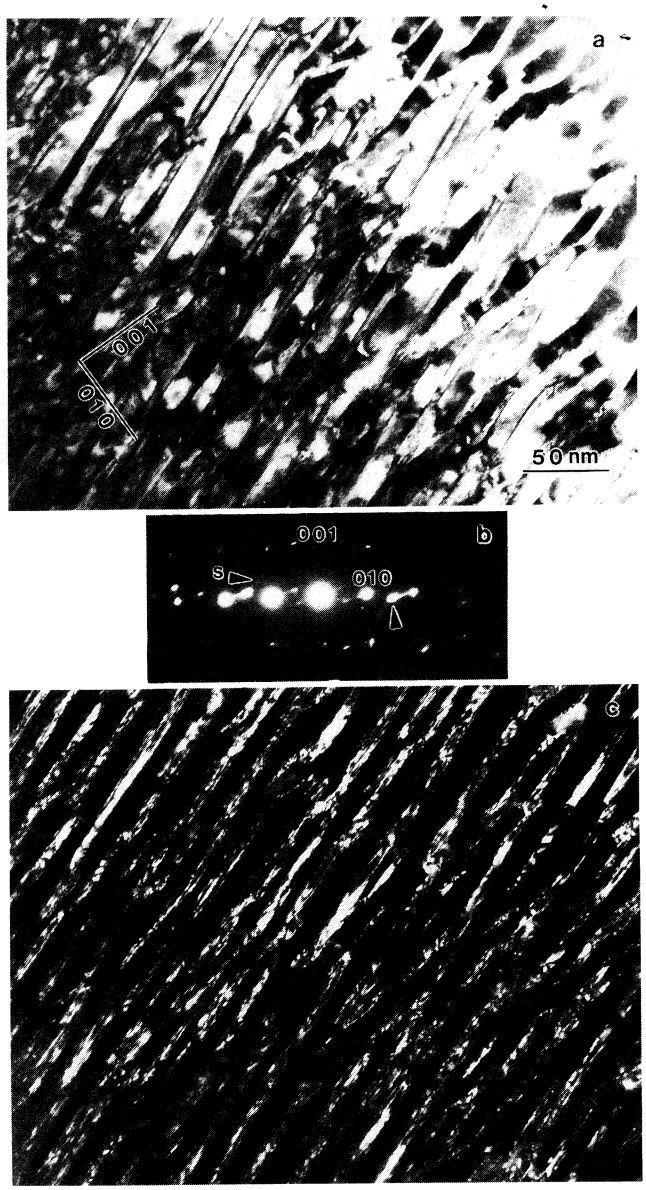

Fig. 5 — TEM photographs taken from an alloy aged at 300 °C for 24 hs. (*a*) BF image. (*b*) Associated SADP. (*c*) DF image taken with the 002 precipitate reflection indicated in (b). In contrast to the sawtooth morphology of the air-cooled alloys, individual precipitate plates, each having a respective habit plane rotated globally over the whole plate, are observed.

such disintegration into different elastic colonies is a manifestation of the tendency to minimize the total elastic energy of a two-phase system and is caused by a strain-induced interaction among precipitate plates in the course of coarsening.[7,9]

As for the details of the individual precipitate plates, a few interesting aspects are found from a comparison of Figures 5 and 6 (each set of TEM photographs were taken under a similar diffracting condition). First, striation contrast inside the plates is observable in the micrographs of both sets, yet it is more prominent in the latter. In particular, much of the striation contrast in Figure 5(a) appears to be characteristic of stacking faults (sharply streaked intensity distribution near the 002 precipitate reflection which is marked **s** is typical of stacking faults[3]).

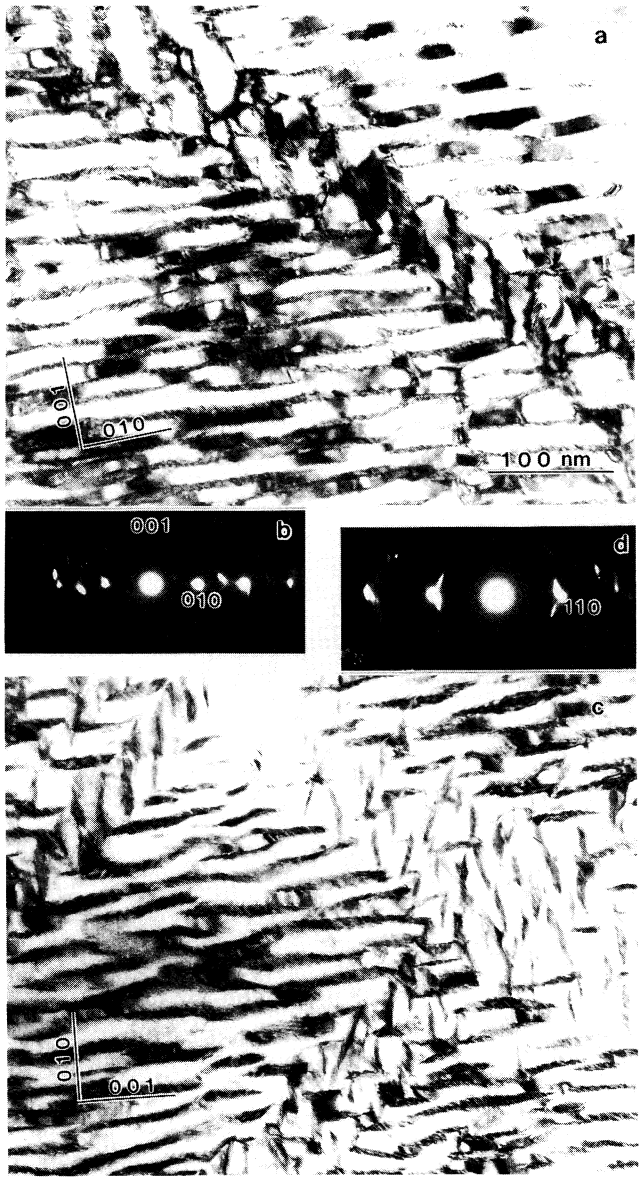

Fig. 6—TEM photographs taken from an alloy aged at 300 °C and for 24 hs. (*a*) and (*c*) BF images. (*b*) and (*d*) Associated SADPs. Notice a characteristic spatial distribution of the precipitate plates forming a macroscopic polytwin configuration.

Second, rotation of the habit planes, and thus of the crystal lattices, is more progressed in the case of Figure 5. Measurement of the angle α, as defined in Figure 4(a), shows that rotation of the 020 precipitate reflection is about 5 deg smaller in Figure 6(b) than in Figure 5(b). From these observations, the following suggestion may be made. The habit plane rotation of an individual precipitate plate and concomitant coarsening may involve the elimination of the twin domains which may come about during earlier stages of coarsening. In view of the long aging time employed, the fine nature of twin domains (Figure 6(a)) and the lack of detectable twin-domain contrast in the pronouncedly rotated precipitate plates (Figure 5) may not be explained unless the formation of the twin domains is in conflict with the global rotation of the habit plane of the plate.

V. DISCUSSION AND CONCLUSIONS

The difference in precipitate morphologies, as described previously, was caused by a change in the kinetic path of the decomposition and is principally related to the difference in relative reaction time in the (bcc + B2) two-phase field. As indicated earlier, a prolonged isostructural decomposition would lead to a significant coarsening of the Cu-rich {001} GP zone plates before their transformation into α' precipitate plates. It is obvious that a global habit rotation of a large α' precipitate plate is not kinetically favorable, since it requires an extensive solute redistribution. In the presence of an effective twin-domain formation mechanism (*i.e.*, plate intersection), it would instead form a polytwin plate and rotate the habit planes segmentwise. The situation is different in the quenched/aged alloys. Very fine precipitate plates, inherited from as-quenched states, are yet to grow and to coarsen as well as to relax the Bain transformation strain during the aging process. One can readily expect that satisfying both these needs while preserving the sawtooth morphology is mechanistically very difficult, and thus, a global rotation of the habit plane would be favored in this case. Understanding that the difference in precipitate morphology is of a kinetic origin, as discussed above, the following questions arise. As compared with the individual precipitate plate with a globally rotated habit plane, what is the nature of the sawtooth-type polytwin plate in terms of the efficacy of the Bain strain relaxation? And, related to this, what could be a reason other than a mechanistic difficulty for the sparsity or the lack of twin domains in a globally rotated precipitate plate? In the following, we attempt to shed some light on these questions by considering the elastic strain energy of a polytwin plate.

The sawtooth morphology of the polytwin plates that we have observed has rarely been discussed. The morphology is different from the theoretical one, not only in terms of its appearance but probably also in its nature.* To be more specific, the morphology may not ensure the fulfillment of the *invariant plane strain* condition, and accordingly, a polytwin plate with the observed morphology may never be in a stress-free state unless its interface with the matrix becomes incoherent. In order to understand this point more clearly, we start with a description of a theoretical morphology of a polytwin plate which is predicted from the elasticity theory of polytwin morphology[9–12] or equivalently from the theories of twinned martensite.[13]

*Despite an ostensible similarity, the morphology is quite different in nature from the "truss shape" polytwin morphology which was discussed in regard to martensite plates in steels.[8]

In order to be consistent with the convention which we used to determine the habit planes, we consider a polytwin plate made up of variants 3 and 2 which have the axes of Bain distortion parallel to $[001]_\gamma$ and $[010]_\gamma$ respectively. For such a polytwin plate, the total stress-free transformation strain is given by

$$\bar{\varepsilon}^0 = z\hat{\varepsilon}^0(3) + (1 - z)\,\hat{\varepsilon}^0(2) \qquad [1]$$

where z is the volume fraction of variant 3 and $\hat{\varepsilon}^0(3)$

and $\hat{\varepsilon}^0$ (2) are the stress-free transformation strain tensors of variants 3 and 2, defined by Eq. [2].

$$\hat{\varepsilon}^0(3) = \begin{pmatrix} \varepsilon_{11}^0 & 0 & 0 \\ 0 & \varepsilon_{11}^0 & 0 \\ 0 & 0 & \varepsilon_{33}^0 \end{pmatrix} \quad \hat{\varepsilon}^0(2) = \begin{pmatrix} \varepsilon_{11}^0 & 0 & 0 \\ 0 & \varepsilon_{33}^0 & 0 \\ 0 & 0 & \varepsilon_{11}^0 \end{pmatrix} \qquad [2]$$

where ε_{11}^0 and ε_{33}^0 are given by Eq. [3] for the Bain distortion considered:

$$\varepsilon_{11}^0 = \frac{a_\alpha - \sqrt{2}\, a_\gamma}{\sqrt{2}\, a_\gamma} \qquad \varepsilon_{33}^0 = \frac{a_\alpha - a_\gamma}{a_\gamma} \qquad [3]$$

where a_α and a_γ denotes the lattice parameters of the stress-free α and γ phases. The volume-dependent elastic strain energy of the polytwin plate, which is characterized by Eq. [2] and by an arbitrary habit normal **n**, is then given in Eqs. [A1] through [A4] with the strain tensor (Eq. [2]) and the corresponding stress tensor substituted. With the resulting expression, the normalized effective strain energy E_{eff} is defined as $E_{\text{eff}} = B(\mathbf{n}, z_{\text{eq}})/C_{11}$ (see Eq. [A2] for $B(\mathbf{n})$), where z_{eq} is such that $B(\mathbf{n}, z)$ is extremized for a given habit normal **n**. The E_{eff} was calculated for different habit normals of the $[h0k]_\gamma$ type ranging from $[001]_\gamma$ to $[101]_\gamma$, and the results are shown in Figure 7 along with the calculated results for a single-domain ($z = 1$) plate. One can see that the strain energy of a polytwin plate is lower than that of a single-domain plate for the entire range of habit normals and that it completely vanishes; (therefore, the invariant plane strain condition is fulfilled) at a particular habit normal ($\mathbf{n}_0$) and for a particular volume fraction (z_0).

Elasticity theories of polytwin morphology and the crystallographic theory of twinned martensite systematically predict $\mathbf{n}_0$ and z_0 based on the concept of invariant plane strain. From the analytic expressions provided by elasticity theories,[9–12] these quantities are found to be $\mathbf{n}_0 = [0.3998, 0, 0.9166]_\gamma // [1, 0, 2.29]_\gamma$ and $z_0 = 0.862$**

**The crystallographic theory of twinned martensite predicts $\mathbf{n}_0 = (0.38581, 0.06385, 0.92037)_\gamma$ and $z_0 = 0.83284$. This discrepancy is due to the small strain approximation employed in the elasticity theory.

($\mathbf{n}_0$ for the single-domain plate at the finite strain energy minimum is $\mathbf{n}_0 = [0.44241, 0, 0.89681]_\gamma // [1, 0, 2.027]_\gamma$). One should notice that this predicted invariant plane normal is different not only from the overall habit ($\sim[001]_\gamma$) but from the segment habit ($(0hk)_\gamma$ type) of the observed sawtooth morphology. This suggests that a polytwin plate with the sawtooth morphology may not fulfill the invariant plane strain condition regardless of the extent of segment rotation. Within the context of the theories, the $(0hk)_\gamma$-type invariant plane can only be attained for a polytwin plate consisting of variants 1 and 3. With variant 2 twin domains present, a sawtooth polytwin plate may only achieve a complete relaxation of strain energy either by the loss of coherency with the matrix or by incorporation of secondary domains (either variant 1 twin domains or stacking faults).

By use of the strain energy expression introduced previously, a calculation was made this time for the different habit normals of the $[0hk]_\gamma$ type ranging from $[001]_\gamma$ to $[011]_\gamma$. The results are summarized in Figure 8. As compared with the previous case, a qualitatively different trend in the variation of the strain energy of a polytwin plate and of the volume fraction of the variant 3 with a change in habit normal can be observed. As the rotation angle (θ) increases, the strain energy of a polytwin plate remains constant while the energy difference (E_{eff} ($z = 1$) − E_{eff} ($z = z_{\text{eq}}$), which is the largest initially at the $[001]_\gamma$ orientation) gradually decreases until it vanishes at the strain energy minimum of a single-domain plate: $\mathbf{n}_0 // [0, 1, 2.027]_\gamma$. Corresponding to this, the volume fraction of variant 3 monotonically increases (the volume fraction of variant 2 decreases) until $z = 1$, where a polytwin plate becomes a single-domain plate. This seems to constitute one of the reasons why variant 2 twin domains were hardly found inside the variant 3 plates with globally rotated habit planes in the quenched/aged alloys.

Quantifying the precise nature of the sawtooth-type polytwin plate beyond the discussions presented above would require a refinement of the physical model of a polytwin plate which was employed in the preceding calculations. It is not explored in the present work. It may

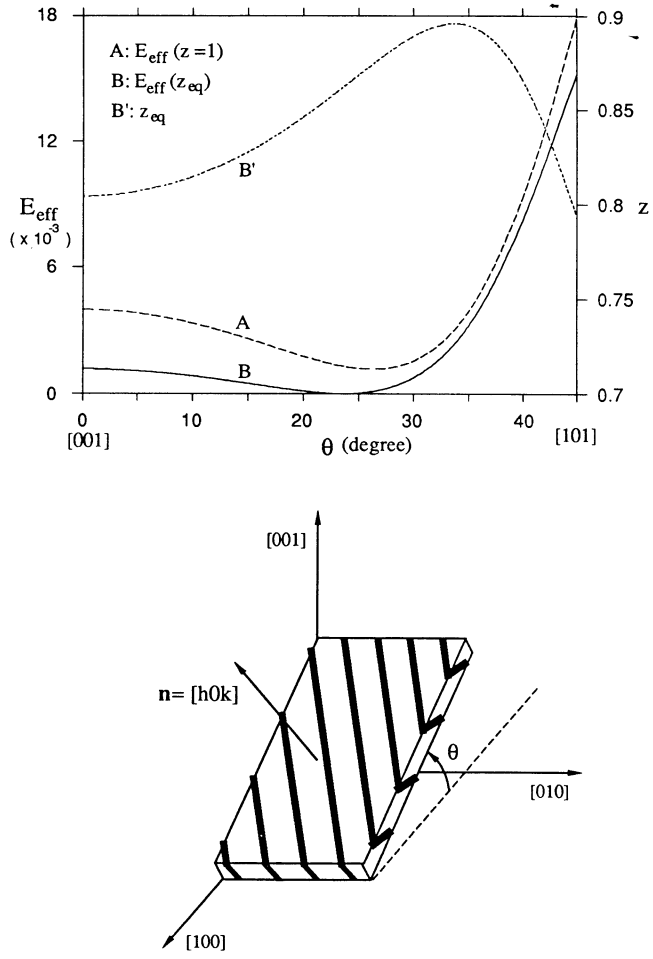

Fig. 7—Calculated elastic strain energy of a polytwin plate consisting of variants 2 and 3 for different habit plane normals of the [h0k] type. Notice that the strain energy of a polytwin plate is lower than that of a single-domain plate for the entire range of habit plane normals and that it completely vanishes at a θ value of $\theta = 23.56$ deg.

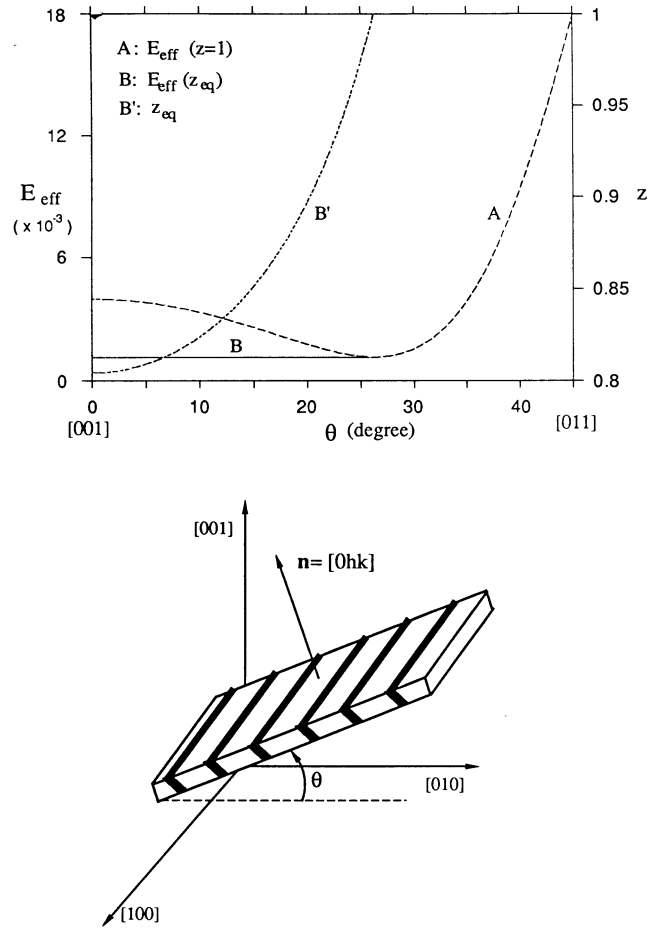

Fig. 8—Calculated elastic strain energy of a polytwin plate consisting of variants 2 and 3 for different habit plane normals of the [0hk] type. Notice that the strain energy of a polytwin plate gradually approaches that of a single-domain plate until the energy difference completely vanishes at the strain energy minimum of a single-domain plate.

suffice to point out as a conclusion that the sawtooth-type polytwin plate is a metastable morphology whose emergence was effected by certain kinetic factors in the presence of an impending need of further relaxation of the Bain strain. As was discussed earlier, these kinetic factors include difficulty of mass transport for a global habit rotation and the intersection among α' plates of different {001} orientations.

APPENDIX

Strain energy of a coherent platelike precipitate

According to Khachaturyan,[9,14] the strain energy of a thin coherent platelike precipitate embedded in an anisotropic infinite matrix is given by Eq. [A1], provided that the precipitate phase has the elastic moduli identical to that of the matrix phase (homogeneous moduli approximation).

$$E = \frac{1}{2} B(\mathbf{n}) V \qquad [A1]$$

where V is the volume of the precipitate and $B(\mathbf{n})$ is given by

$$B(\mathbf{n}) = \lambda_{ijkl}\, \varepsilon^0_{ij}\, \varepsilon^0_{kl} - n_i\, \sigma^0_{ij}\, \Omega_{jl}\, \sigma^0_{lm}\, n_m \qquad [A2]$$

where $\mathbf{n} = \mathbf{k}/k$, λ_{ijkl} is the elastic modulus tensor, ε^0_{ij} is the strain tensor describing the geometrical difference between the crystal lattices of the matrix and the precipitate phase in their respective stress-free state, and σ^0_{ij} and Ω_{ij} are tensors given by

$$\sigma^0_{ij} = \lambda_{ijkl}\, \varepsilon^0_{kl} \qquad [A3]$$

$$\Omega^{-1}_{ij} = \lambda_{ikjl}\, n_k\, n_l \qquad [A4]$$

If multiplied by one-half, the first term in $B(\mathbf{n})$ represents the strain energy arising from the stress-free transformation into a unit volume of the precipitate, and the negative second term represents the strain energy associated with the relaxation of the stress-free transformed volume of the precipitate through coherency with the matrix. Accordingly, $B(\mathbf{n})$ is positive semidefinite, since otherwise, a nonphysical matrix state is encountered where the matrix has a negative resistance to the relaxation of the precipitate.

ACKNOWLEDGMENT

The authors gratefully acknowledge BrushWellman Inc. for a fellowship and for providing the CuBe alloys.

REFERENCES

1. T. Tadaki, T. Sahara, and K. Shimizu: *Trans. Jpn. Inst. Met.*, 1973, vol. 44, pp. 401-07.
2. X. Auvray: Sc.D. Thesis, University of Rouen, France, 1977.
3. B. Cheong, K. Hono, and D.E. Laughlin: Carnegie Mellon University, Pittsburgh, PA, unpublished research, 1993; B. Cheong: Ph.D. Thesis, Chapter 5, Carnegie Mellon University, Pittsburgh, PA, 1992.
4. D.J. Chakrabarti, D.E. Laughlin, and L.E. Tanner: *Bull. Alloy Phase Diagrams*, 1987, vol. 8, pp. 269-82.
5. S.M. Allen and J.W. Cahn: *Acta Metall.*, 1976, vol. 24, pp. 425-37.
6. A.G. Khachaturyan and D.E. Laughlin: *Acta Metall.*, 1990, vol. 38, pp. 1823-35.
7. S.H. Wen, A.G. Khachaturyan, and J.W. Morris, Jr.: *Metall. Trans. A*, 1981, vol. 12A, pp. 581-87.
8. A.L. Roitburd: *Sov. Phys. Solid State*, 1969, vol. 11, pp. 1191-98.
9. A.G. Khachaturyan: *Theory of Structural Transformations in Solids*, John Wiley & Sons, New York, NY, 1983.
10. A.G. Khachaturyan and G.A. Shatalov: *Sov. Phys. JETP*, 1969, vol. 29, pp. 557-61.
11. A.L. Roitburd: *Sov. Phys. Solid State*, 1969, vol. 10, pp. 2870-76.
12. A.L. Roitburd: *Phys. Status Solidi*, 1973, vol. 16 (a), pp. 329-38.
13. M.S. Wechsler, D.S. Lieberman, and T.A. Read: *TMS-AIME*, 1953, vol. 197, pp. 1503-15.
14. A.G. Khachaturyan: *Sov. Phys. Solid State*, 1967, vol. 8, pp. 2163-68.